Applied Surface Science 363 (2016) 372–380

Contents lists available at ScienceDirect

Applied Surface Science

journal homepage: www.elsevier.com/locate/apsusc

Adsorption and subsequent partial photodegradation of methyl violet 2B on Cu/Al layered double hydroxides

Ariel Guzmán-Vargas[a,*], Enrique Lima[b], Gisselle A. Uriostegui-Ortega[a], Miguel A. Oliver-Tolentino[c], Esaú E. Rodríguez[d]

[a] Instituto Politécnico Nacional, ESIQIE-SEPI-DIQI, Laboratorio de Investigación en Materiales Porosos, Catálisis Ambiental y Química Fina (LiMpCa-QuF), UPALM Edif. 7 P.B. Zacatenco, GAM, México, D.F.07738, Mexico

[b] Instituto de Investigaciones en Materiales-UNAM, Circuito exterior s/n, Cd. Universitaria, Del. Coyoacán, México, D.F. 04510, Mexico

[c] Instituto Politécnico Nacional, Centro de Investigación en Ciencia Aplicada y Tecnología Avanzada, Calzada Legaria 694, Col. Irrigación, México, D.F. 11500, Mexico

[d] Departamento de Química, Centro de Investigación y de Estudios Avanzados del Instituto Politécnico Nacional, Av. Instituto Politécnico Nacional 2580, Col. San Pedro Zacatenco, México, D.F. 07360, Mexico

ARTICLE INFO

Article history:
Received 19 September 2015
Received in revised form 3 December 2015
Accepted 6 December 2015
Available online 11 December 2015

Keywords:
LDH Cu/Al materials
Adsorption models
Photodegradation
characterization
MV dye
Kinetic

ABSTRACT

Uncalcined Cu/Al LDH was studied as adsorbent and photocatalyst in the adsorption and subsequent photodegradation of methyl violet 2B dye (MV2B). Physicochemical characterization was carried out by XRD, FTIR, UV–vis, including photoactive properties, DSC/TGA and SEM. Kinetic and thermodynamic models showed great affinity and sorption capacity, the maximum adsorption capacity was 361.0 mg g^{-1} obtained by Langmuir model, in addition, the results showed that the dye was adsorbed on the LDH surface. Photocatalytic activity was evaluated in the MV2B dye photodegradation process, and it was confirmed by the presence •OH radicals monitored by EPR spin trapping technique, additionally, COD and TOC parameters were measured, ^{13}C NMR showed differences for the adsorbed and photodegraded samples.

1. Introduction

The textile industry is one of the largest polluters in the world. It is estimated that close to 20% of global industrial water pollution comes from the treatment and dyeing of textiles [1]. In this context, during the coloration process a large percentage of the synthetic dye is transferred to the waste stream. Thus, dyes can be released into the environment making the effluent a pollution source. Dyes are difficult to remove in conventional water treatment procedures and can be transported easily through water bodies such as rivers [2,3]. One of most common dye used in color industry is the Methyl violet 2B (MV2B), which is a basic dye [4,5]. MV2B dye is a typical aromatic azo compound with molecular formula $C_{24}H_{28}ClN_3$. Its structure is shown in inset of Fig. 1B. MV2B find applications in non-linear optics [6], gamma radiation sensors [7], ink colorant [8] and dye sensitized solid state photovoltaic cells [9].

It is well known that methyl violet could delay the growth of bacteria and photosynthesis of aquatic plants. This dye is potentially carcinogenic and may be harmful by ingestion, inhalation and skin contact. Because of these harmful properties of this dye, it has to be removed from industrial wastewater before being discharged into the environment [10,11]. The strategies to accomplish this challenge include removal by filtration or other physical methods that are particularly difficult to achieve because of solubility of dyes [12,13]. Some alternatives to remove this type of effluent involve the destruction of the pollutant molecules by means of chemical reactions or their retention in inorganic matrices [14]. The selection of an adsorbent depends on the physicochemical properties of the molecule to be removed. For example, the acidity and size windows of some molecular sieves are suitable for encapsulation of thioindigo molecules [15]. In other cases, layered double hydroxides (LDH), otherwise known as hydrotalcite-like compounds, are anionic exchangers and, therefore, able to retain anionic dyes. LDH not only adsorb anionic species, they are also able to retain neutral molecules. The structural and surface properties of LDH are suitable for trapping some molecules with polar bonds [16].

Layered double hydroxides result from the association of divalent (Mg^{2+}, Zn^{2+}, Ni^{2+}, Co^{2+}, etc.) and trivalent (Al^{3+}, Cr^{3+}, Fe^{3+}, etc.) metal ions placed in the center of octahedral units. On the edges of

* Corresponding author.
E-mail address: aguzmanv@ipn.mx (A. Guzmán-Vargas).

http://dx.doi.org/10.1016/j.apsusc.2015.12.050
0169-4332/

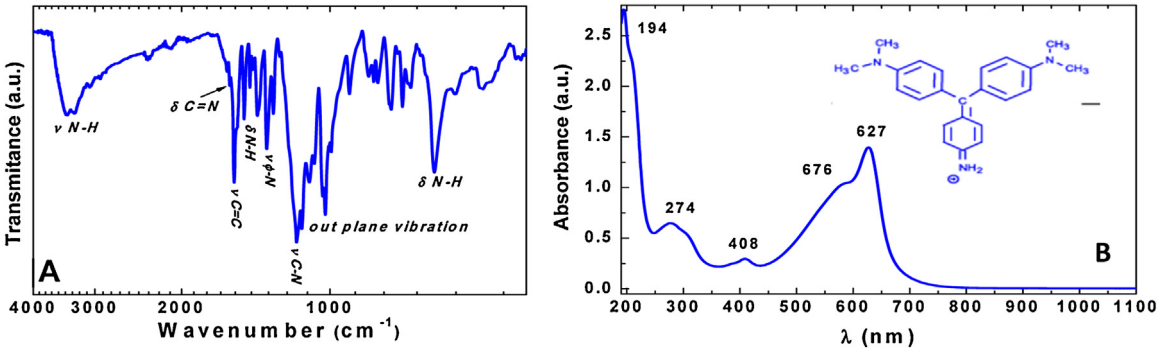

Fig. 1. Spectra of MV2B: (A) IR solid dye, (B) UV–vis in solution, inset: chemical dye structure.

octahedra, hydroxyl groups are placed. These octahedra units are joined to form a lamellar structure mimic that of brucite-like layers, the presence of both divalent and trivalent metals in layers results in a positive charge, which is balanced by intercalation of anions (Cl^-, NO_3^-, CO_3^{2-}, SO_4^{2-}) and water between the layers [17]. LDH can be represented by the general formula:

$$[M^{II}_{1-x}M^{III}_{x}(OH)_2]^{x+}[A^{n-}_{x/n}]\cdot mH_2O$$

Due to the wide range of chemical composition where LDHs can be obtained, their physicochemical properties are easily tuned [18,19], which have been enabled to use them in different areas, as catalysis [20], electrocatalysis [21,22], energy storage [23], photocatalysis [24], adsorption [25], and films/coatings for protection [26–28] among others. In particular, the copper-containing hydrotalcites represent a rather unusual system within this family of compounds, due to the well-known tendency of copper to form distorted octahedra because of the Jahn–Teller effect. Consequently, much effort has been made to prepare hydrotalcites containing copper, to be used for different purposes; for instance, LDH Cu–Mg/Al has been used as catalyst in the selective oxidation of biorenewable glycerol and in NO_x removal [29]. LDH Cu/Al has shown magnetic properties [30] and recently, thermal properties were attribute to the nanofluid behavior in the preparation method [31]. Other systems, like LDH Cu/Fe and Cu/Al have been used as adsorbent of organic compounds from aqueous media [32,33]. Photocalytic conversions of carbon dioxide into methanol using LDH Zn–Cu/Al and photocatalysis in aqueous media with LDH Cu/Cr are also been reported [34,35].

Thus, in this work the LDH Cu/Al was evaluated as an adsorbent and photocatalyst for degradation of methyl violet 2B dye (MV2B).

2. Experimental

2.1. Materials

The LDH Cu/Al was obtained by coprecipitation method at pH 8.3 as described elsewhere. Briefly, three solution were prepared, solution A (NaOH 1 mol L^{-1}), solution B (Na_2CO_3 0.25 mol L^{-1}) and solution C ($Al(NO_3)_3$ 0.44 mol L^{-1} and $Cu(NO_3)_2{\cdot}2.5H_2O$ 0.78 mol L^{-1}). 25 mL of solution B was kept under vigorous stirring; the solution A was slowly added until reach a pH 8.3, this pH was maintained by addition of solution A while solution C was added to solution B. After complete addition of solution C the resultant slurry was stirred for 1 h at room temperature; then the solid obtained was separated by centrifugation, rinsed thoroughly with warm distilled water, and dried overnight at 80 °C.

Commercial Methyl violet 2B (MV2B) dye was provided by Roshfrans company, it was employed as received.

2.2. XRD, FT-IR, UV–vis, thermal and SEM analysis

The structural characterization of adsorbent was performed by X-ray diffraction (XRD), infrared, ultraviolet-visible and nuclear magnetic resonance spectroscopies. XRD patterns were acquired using a Philips X'PERTPRO instrument operating with CuKα1 radiation (λ = 1.542 Å, 45 kV, and 40 mA); The FTIR spectra were recorded in a spectrophotometer Perkin Elmer RX-1, operating in attenuated total reflectance mode (ATR); UV–vis-NIR spectra were recorded in a spectrophotometer Perkin Elmer Lambda 950. Solid state nuclear magnetic resonance (MAS NMR) measurements were performed in an Avance-400 Bruker (9.39 T) spectrometer. ^{13}C CP MAS NMR spectra were acquired when the spectrometer was operated at a resonance frequency of 100.2 MHz, with contact time of 1 ms at 5 kHz spinning rate, and 90° pulses of 4 ms, at least 20,000 scans were made. Chemical shifts were referenced to solid CH_2 adamantane shift at 38.2 ppm relative to TMS. The thermal analysis was carried out in a Perkin Elmer STA 6000 (DSC/TGA) apparatus. 5 mg of sample were heated from room temperature to 700 °C (ramp = 10 °C min^{-1}) in a nitrogen flow of 40 mL min^{-1}. Scanning electron microscopy (SEM) images of the samples were taken on a microscope BENCHTOP JCM-6000 equipped with energy-dispersive X-ray (EDX) facility. The samples were coated with gold using sputter coating to avoid charging. Analysis was carried out at an accelerating voltage of 15 kV.

2.3. Adsorption and photodegradation measurements

The MV2B adsorption experiments on LDH Cu/Al were carried out in a glass reactor (batch operation) at room temperature and atmospheric pressure. Typical run adsorption conditions were as follows: 60 mg of LDH were dispersed in 60 mL of MV2B aqueous solution at different concentrations (50, 75, 100 and 200 mg L^{-1}) at pH 7–8. The suspension was kept under vigorous agitation; in order to prevent sunlight interact with suspension the reactor was kept in dark. The reaction evolution, sampling over the time, was followed by UV–vis spectroscopy. The absorbance was measured at the wavelength of 627 nm.

The photocatalytic experiments were conducted after the adsorption equilibrium was reached (120 min) using a UV light power source at 365 nm (4 W). The reaction evolution, sampling over the time, was followed by chemical oxygen demand (COD) removal parameter which was measured in a Hacht apparatus employing Hanna kits (HI93754C certified COD reagents) and total organic carbon (TOC) which was measured in TOC-V-CSN equipment.

2.4. Electron paramagnetic resonance (EPR) experiments

EPR spectroscopy (spin trapping technique) was employed to verify the formation of •OH radicals. Samples were analyzed

at room temperature using X-band EPR (9.8 GHz), spectra were collected using an EMX Plus Bruker System, with an ER 041 XG microwave bridge and an ER 4102ST cavity. The following conditions were used: 4096 points; microwave power, 20 mW; modulation amplitude, 4 G; modulation frequency, 100 kHz; time constant, 327 ms; conversion time, 8 ms; and averaging over 2 scans. DMPO, 5,5-Dimethyl-1-pyrroline N-oxide, was purchased from D5766 Sigma–Aldrich, with purity ≥97%, it was used as radicals spin-trapped.

3. Results and discussion

3.1. Dye

The FT-IR spectra of MV2B powder is exhibited in Fig. 1A. The absorption bands at 3072 cm^{-1}, 1171 cm^{-1} (υ C—H), 1567 cm^{-1} (υ C=C) and 800 cm^{-1} (δ C—H) are characteristic of aromatic compounds; the vibrations associated to aliphatic groups in the MV2B are responsible of the bands at 497 cm^{-1} (υ C—C), 1625 cm^{-1} (υ C=C), 2856 cm^{-1} (υ_{sym} C—H), 2925 cm^{-1} (υ_{asym} C—H), 1457 cm^{-1} (δ_{asym} C—H) and 1342 cm^{-1} (δ_{sym} C—H); whereas, the presence of amine group results in the bands around 3500 cm^{-1} (υ N—H), 1300 cm^{-1} (υ C_{arom}—N), 1104 cm^{-1} (υ C_{aliph}—N), 3493 cm^{-1} (υ N—H), 3303 cm^{-1} (υ C=N), 1600 cm^{-1} (δ N—H) and 619 cm^{-1} (associated to torsional vibration) [24]. This compound in solution exhibited two absorption bands in the UV spectral window (Fig. 1B), the bands at 194 and 274 nm are attributed to electronic transition $\pi \rightarrow \pi^*$ for aromatic ring and $n \rightarrow \pi^*$ for C=N, while in the visible region presented three bands 408, 575 and 627 associated to chromophore groups; especially the band 627 nm has been assigned to the simultaneous adsorption phenomena due to (i) a trap level near the LUMO band and (ii) a charge transfer resonance between the HOMO level [36,37]. The MV2B structure is shown in the inset of Fig. 1B.

3.2. Layered double hydroxides Cu/Al

Lamellar structure of LDH was confirmed by X-ray diffraction. The powder X-ray diffractogram of the synthesized LDH is shown in Fig. 2A. The pattern matched to that of a hexagonal lattice with R3m rhombohedral symmetry (JCPDS card 22-0700); the calculated cell parameters from X-ray data and the molar ratio between M^{II}/M^{III} are listed in Table 1.

The corresponding FT-IR spectrum is exhibited in the inset of Fig. 2A. The intense and broad lines are observed between 3416 and 3388 cm^{-1} and ascribed to the O—H stretching vibration mode of water molecules, which are intercalated in the interlayer space.

Besides, water molecules, hydrogen-bonded hydroxyl groups along the cationic sheets are also responsible for broadening of the band. The medium-intensity band around 1735 cm^{-1} is related to the bending mode of water molecules (δ_{H_2O}). The stretching mode of CO_3^{2-} anions is responsible for the sharp and strong band around 1362 cm^{-1}. The stretching and bending vibrational modes associated to hydroxometallic octahedral complexes, which constitute the $[M^{II}{}_{1-x}M^{III}{}_x(OH)_2]^{x+}$ cationic brucite-like sheets, are responsible for absorption at lower wavenumbers (<800 cm^{-1}) [38].

The UV–vis spectrum of LDH Cu/Al is showed in the Fig. 2B, two types of bands were identified: ligand-to-metal charge-transfer (LMCT) band in the 350–200 nm range and d–d transition bands in the 850–600 nm range, this d–d transition is associated to $^2E_g(D) \rightarrow {}^2T_{2g}(D)$, which is expected transition for Cu^{2+} in a distorted – six-fold coordination with octahedral arrangement, as occurs in the LDH framework due to Jahn–Teller effect [39]. It is well-known that light absorption by the materials and the migration of the light-induced electrons and holes are the key factors controlling a photocatalytic reaction which is relevant to the electronic structure of the material. In principle, the photo absorption of the photocatalyst depends on the mobility of electron–hole pairs, which determine the probability of electrons and holes to reach reaction sites at the surface of the photocatalyst. The photoabsorption properties of the LDH material detected by UV–vis are illustrated in Fig. 2C.

For a crystalline semiconductor, the optical bandgap is determined by the following equation using the optical absorption data near the band edge [40]:

$$(\alpha h\upsilon)^2 = A(h\upsilon - E_g) \quad (1)$$

where α, υ, A, and E_g are the absorption coefficient, light frequency, proportionality constant, and band gap, respectively. However, when the material scatters in a perfectly diffuse manner following expression can be used:

$$[F(R)h\upsilon]^2 = B(h\upsilon - E_g) \quad (2)$$

where $F(R)$ is the so-called remission or Kubelka–Munk function and B is proportionality constant. Therefore, plotting $[F(R)h\nu]^2$ against $h\nu$, the band gap E_g of a sample can be determined by extrapolating the linear region of the plot to zero absorption, the value obtained is reported in Table 1.

In order to verify that the LDH Cu/Al exhibits semiconductor properties, electrochemical experiments were carried out. Fig. 2D includes results of measurements of temporal transients of open-circuit potential (E_{OCP}–t) applied to the electrode–electrolyte interface which indeed are a sensitive resource for a major understanding on the behavior of electrochemical phenomena with regard to light excitation at semiconductor materials. The initial seconds in this figure corresponds to the OCP variation under dark conditions. Note that, after turn-on the UV-lamp a drastic modification of potential toward more negative values was evident. When the lamp is turned-off, the corresponding EOCP transient tended to reach the initial value. The decrease in OCP was due to the generation of electron–hole pairs that leaded to changes in the flat band potential and, therefore, to a decrease in the OCP down to more negative potentials. In fact, the potential decay allows evaluating the hole and electron reactivity and, therefore, the potential efficiency of the photocatalyst [41].

3.3. MVB adsorption

3.3.1. Adsorption uptakes

The effect of contact time between MV2B and 60 mg of LDH Cu/Al was studied in different solutions where the concentration of the dye was 50, 75, 100 or 200 mg L^{-1}; the experiments were monitored for 270 min. Fig. 3A shows that a large amount of MV2B remained adsorbed onto LDH Cu/Al after a very short contact time.

Uptake of MV2B, Q_e (mg g^{-1}), by LDH adsorbent was calculated using the relation:

$$Q_e = \frac{(C_0 - C_t)V}{M} \quad (3)$$

where C_0 and C_t (mg L^{-1}) being the initial concentration of MV2B and concentration at time t in solution, V being the volume of the solution (L) and M the mass of dry adsorbent (g).

The results are presented in Fig. 3B. It is remarked that the Q_e (adsorbed amount of MV2B at time t) increases rapidly in the first 15 min. The initial removal of MV2B from aqueous solution is a

Table 1
Molar ratio, cell parameters and bandgap of LDH Cu/Al material.

Sample	M^{II}/M^{III} ratio	d_{003} (Å)	a (Å)	c (Å)	E_g (eV)
LDH Cu/Al	3.0	7.55	3.08	22.65	2.85

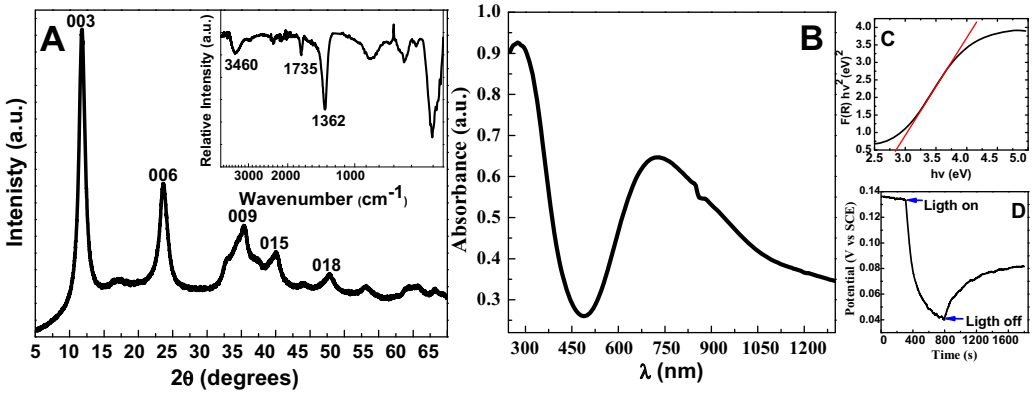

Fig. 2. LDH Cu/Al analysis results: (A) XRD pattern, inset: IR spectrum, (B) diffuse reflectance UV–vis spectrum, (C) $[F(R)h\nu]^2$ versus photon energy plot and (D) E_{ocp}-t experiments.

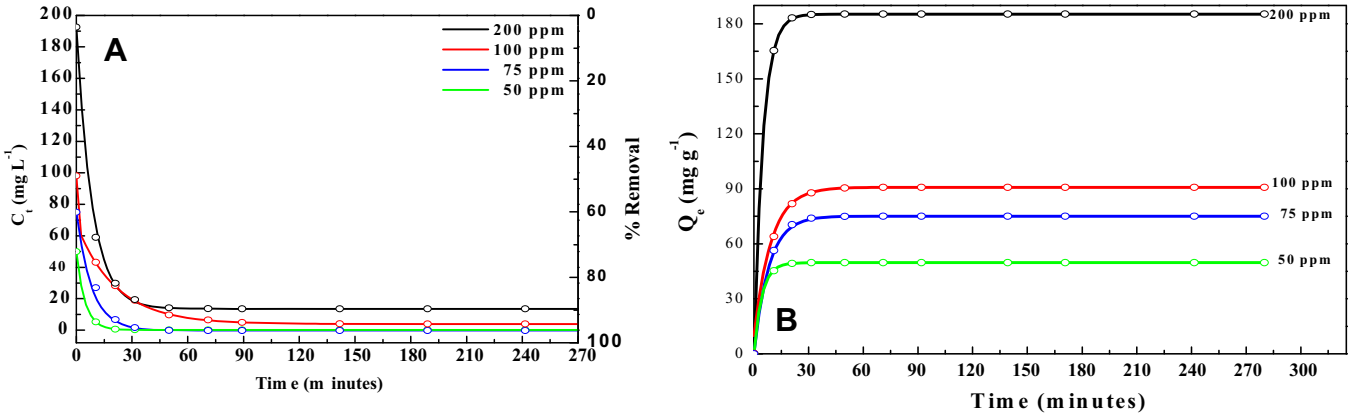

Fig. 3. (A) Concentration profiles of MV2B as a function of time during adsorption and (B) Adsorbed amount of methyl violet as a function of time at different concentrations.

rapid process, where, more than 90% of the dissolved MV2B being removed within only 15 min, so that; an equilibrium adsorption state was reached after 100 min (removal percentage higher than 95%).

3.3.2. Kinetics sorption model

Several steps can be used to express the mechanism of solute sorption onto a sorbent. In order to investigate the mechanism of sorption, various kinetics models, namely, the pseudo-first-order, the pseudo-second-order, the Elovich and the intra-particle diffusion kinetic models, were tested [42].

The linear form of pseudo-first order equation of Lagergren is expressed as follows:

$$log\,(Q_e - Q_t) = \log\, Q_e - \frac{K_1}{2.303}t \tag{4}$$

where Q_e is the amount of dye sorbed at equilibrium in mg g^{-1}; Q_t is the amount of dye sorbed at time t in mg g^{-1}; K_1 is the equilibrium rate constant of pseudo-first sorption in min^{-1}.

In order to obtain the rate constants, the straight line plots of log $(Q_e - Q_t)$ against t for different concentration of MV2B.

The linear form of pseudo-second order equation is the following:

$$\frac{t}{Q_t} = \frac{1}{K_2 {Q_e}^2} + \frac{1}{Q_e}t \tag{5}$$

where K_2 is the equilibrium rate constant of pseudo-second order sorption in g mg^{-1} min^{-1}. The straight line plots of t/Q_t against t have also been tested to obtain rate parameters.

The simplified Elovich equation can be represented as follow:

$$Q_t = \beta \ln(\alpha\beta) + \beta \ln t \tag{6}$$

where α is the initial dye sorption rate in mg g^{-1} min^{-1} and β is the desorption constant in g mg^{-1}. Thus, the constants can be obtained from the slope and intercept of the linear plot of Q_t versus ln t.

The intraparticle diffusion equation is the following:

$$Q_t = K_i t^{0.5} \tag{7}$$

where K_i is the intraparticle diffusion rate constant, mg g^{-1} min$^{-0.5}$. The K_i values are calculated from the slope of the straight line.

The kinetics parameters and correlation coefficients, R^2, values of dye adsorption varying the dye concentration are reported in Table 2. These values show the data-fits had extremely high

Table 2
Kinetic values of adsorption from different models.

Kinetics model	50 (mg L^{-1})	75 (mg L^{-1})	100 (mg L^{-1})	200 (mg L^{-1})
Pseudo first-order				
K_1 (min^{-1})	0.2326	0.1224	0.1074	0.2044
R^2	0.985	0.983	0.988	0.982
Pseudo second-order				
K_2 (g mg^{-1} min^{-1})	1.1×10^{-5}	6.3×10^{-6}	3.4×10^{-6}	2.2×10^{-7}
R^2	0.999	0.999	0.999	0.999
Elovich equation				
α (mg g^{-1} min^{-1})	34.38	3.30	3.39	4.65
β (g mg^{-1})	0.077	0.041	0.038	0.020
R^2	0.854	0.867	0.852	0.846
Intraparticle diffusion				
K_i (mmol g^{-1} min$^{-0.5}$)	0.028	0.042	0.046	0.105
R^2	0.803	0.813	0.807	0.805

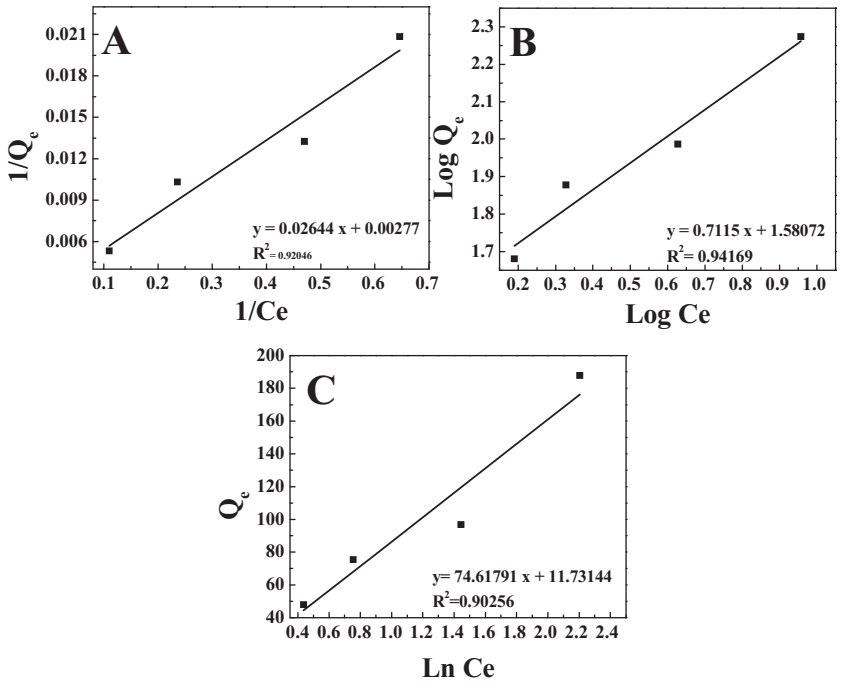

Fig. 4. Adsorption isotherm models: (A) Langmuir, (B) Freundlich and (C) Temkin.

correlation coefficients (R^2 = 0.999) when the pseudo-second order equation was employed. The pseudo-second order model is based on the adsorption loading of the solid phase and predicts the behavior over the whole range of the adsorption process; where the rate constant K_2 decreases with increasing concentration of MV2B in solution.

3.3.3. Thermodynamic parameters

The adsorption isotherms, varying the initial dye concentration, were tested to match with three common adsorption models: Langmuir, Freundlich, and Temkin (Fig. 4) [43].

The Langmuir isotherm equation is based on the physical hypothesis that the maximal adsorption capacity consists of a monolayer adsorption onto an outer surface of the adsorbent, which contains a finite number of identical sites and there are no interactions between adsorbed molecules. Based upon these assumptions, the linear form of Langmuir equation can be represented as follows:

$$\frac{1}{Q_e} = \frac{1}{Q_o} + \frac{1}{Q_o K_L C_e} \tag{8}$$

where C_e is the equilibrium concentration of adsorbate (mg L^{-1}), Q_e is the amount of dye adsorbed per gram of the adsorbent at equilibrium (mg g^{-1}), Q_o is the maximum monolayer coverage capacity (mg g^{-1}) and K_L is the Langmuir isotherm constant (L mg^{-1}). The plot of $1/Q_e$ versus $1/C_e$ will gives a straight line of slope $1/Q_o$ and intercept of $1/K_L Q_o$. The values obtained are showed in Table 3.

Table 3
Thermodynamic parameters from adsorption isotherms.

Langmuir			
Q_O (mg g^{-1})	K_L (L mg^{-1})	R_L	R^2
361.0	0.1047	0.087	0.92046
Freundlich			
$1/n$	n	K_F (mg g^{-1})	R^2
0.7115	1.405	38.082	0.94169
Temkin			
A_T (L g^{-1})	b_T	B (J mol^{-1})	R^2
1.17	32.774	76.61	0.90256

The R_L value indicates that the equilibrium sorption was favorable; with maximum monolayer coverage capacity (Q_o) of 361.0 mg g^{-1} (0.361 g g^{-1}).

The Freundlich adsorption isotherm is commonly used to describe the adsorption characteristics for the heterogeneous surface. The Freundlich isotherm does not predict any saturation of the adsorbent by the adsorbate and assumes that if the concentration of solute in the solution at equilibrium, C_e is the equilibrium concentration of adsorbate (mg L^{-1}), n is the amount of solute adsorbed, Q_e is the amount of dye adsorbed per gram of the adsorbent at equilibrium (mg g^{-1}) and K_f is Freundlich isotherm constant. The linear Freundlich adsorption isotherm can be expressed by the following equation:

$$\log Q_e = \log K_f + \frac{1}{n}\log C_e \tag{9}$$

The Freundlich model permit verify a thermodynamically favorable adsorption of MV2B onto the LDH Cu/Al surface as the Freundlich constant n is greater than 1.

The Temkin isotherm contains a factor that explicitly taking into the account of adsorbent–adsorbate interactions. By ignoring the extremely low and large value of concentrations, this model assumes a uniform distribution of binding energies between the molecules adsorbed and adsorbent. Plotting the amount adsorbed Q_e against $\ln C_e$ is possible obtained the constants from the slope and intercept according to the following model:

$$Q_e = B \ln A_T + B \ln C_e \tag{10}$$

where A_T is Temkin isotherm equilibrium binding constant (L g^{-1}) and B is constant related to heat of sorption (J mol^{-1}). From this model, the following values were estimated A_T = 1.17 L g^{-1} and B = 76.61 J mol^{-1}, which is an indication of the heat of sorption indicating a physical adsorption process.

The next lines are in order to discuss our results vis a vis another studies, involving MV dye adsorption on different materials, for example, Dogan et al. [44] reported that the adsorption onto perlite is favored with the temperature and pH, the process is controlled by the diffusion. Azizian et al. [45] obtained a 0.095 g g^{-1} as maximum

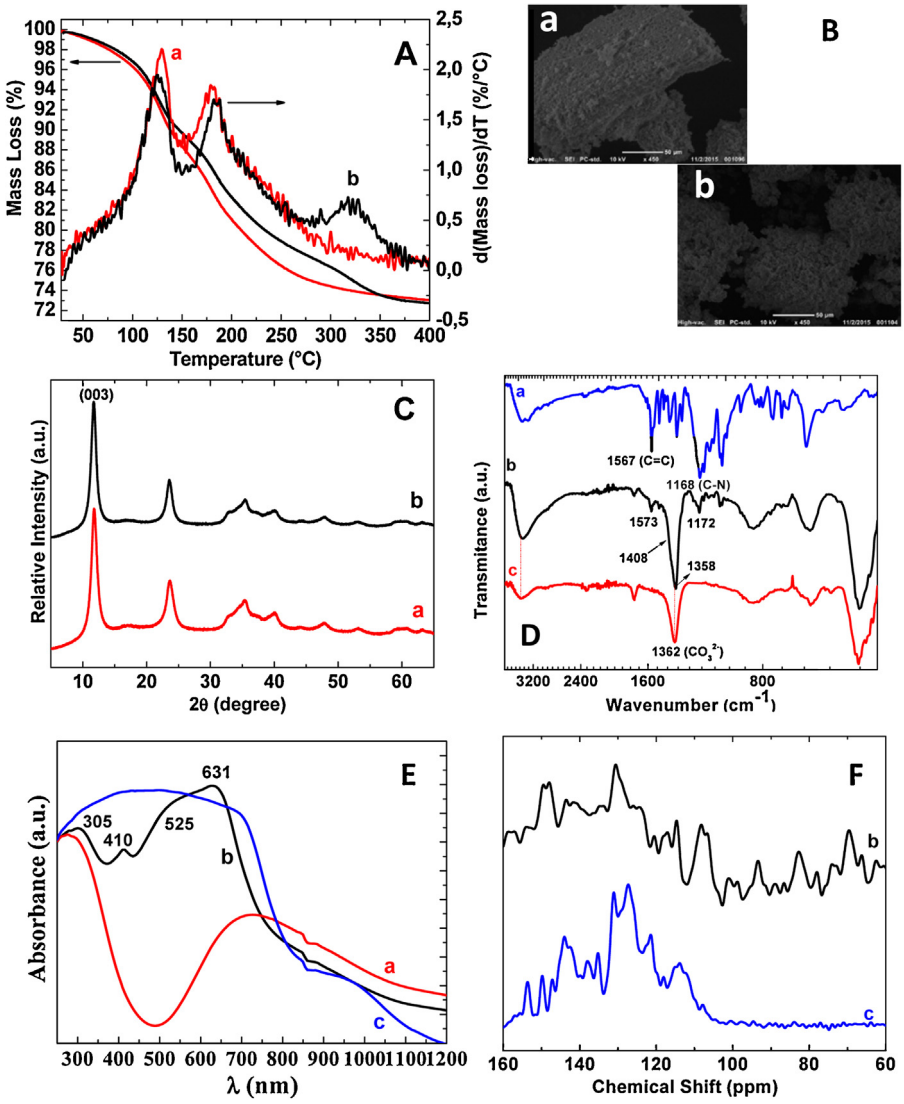

Fig. 5. (A) Thermal analysis, (B) SEM images, (C) XRD patterns, (D) IR spectra, (E) diffuse reflectance UV–vis spectra and (F) ^{13}C NMR of: (a) LDH Cu/Al, (b) MV2B adsorbed on LDH Cu/Al and c) MV2B dye.

adsorption capacity using granular activated carbon. On the other hand, the NiAl-LDH possessing hierarchically porous nanoarchitectures showed the maximum p-nitrophenol adsorption capacity of 77.7 mg g^{-1} (0.0777 g g^{-1}) reported by Sun et al. [25]. Our result is in the same range for calcined Fe–Mg LDH in the adsorption of orange G, exhibiting a maximum sorption capacity of 0.3788 g g^{-1} [46], considering these results, it is clear that the LDH Cu/Al material is a good candidate to be used as sorbent.

Whit the purpose of evaluates some physical characteristics before and after adsorption, thermal and SEM studies were performed. Thermal Analysis profiles (TGA) for LDH Cu/Al as prepared and with MV2B adsorbed are shown in Fig. 5A, three main region are shown from 40 to 400 °C. The first from 40 to 150 °C, for LDH Cu/Al the peak observed around 129 °C (the peaks were obtained from first derivate), corresponds to the around 12% of mass loss in the TGA curve, which was related to the desorption of the physically absorbed water into LDH layers, while for the LDH Cu/Al with MV2B adsorbed, the desorption temperature shifted to 124 °C. In the second region from 150 to 280 °C, the weight loss was about 15 and 10% for the as prepared sample and adsorbed one respectively, the peak ca. 180 °C is assigned to the desorption of interlayer water of LDH [47]; for the adsorbed sample shifts to 184 °C, this fact can be associated to the water interaction with the layer and dye. In the last region from 280 to 400 °C, clearly only one peak appears ca. 322 °C and is assigned to the weight loss of MV2B adsorbed on the LDH (nearly 6%) because for LDH Cu/Al any change was detected, the amount of dye adsorbed calculated from TGA was 350 mg g^{-1} of solid. Up to 350 °C appears the weight loss (not shown) associated to the decarbonatation, dehydroxylation and mixed oxides formation [48].

Concerning to the morphology from SEM images, LDH Cu/Al shows platelet form particles (Fig. 5A) while a change in the surface morphology was observed in the LDH Cu/Al after adsorption process producing flake shape aggregates (Fig. 5B).

The MV2B-LDH Cu/Al interaction upon the adsorption process is in line with the following, explanation. From the maximum diffraction of plane 003 (Fig. 5C), is possible to conclude that the interlamellar space of LDH was not modified as a consequence of the MV2 V adsorption, therefore the dye was not intercalated between the layers, probably interacting with Al^{3+} cations which commonly are present at surface and have a higher polarizing power than Cu^{II} ones. IR results (Fig. 5D) showed that the band due to C=C in the aromatic ring was shifted 9 cm^{-1} towards higher wavenumber when dye is adsorbed on HDL, meaning that main

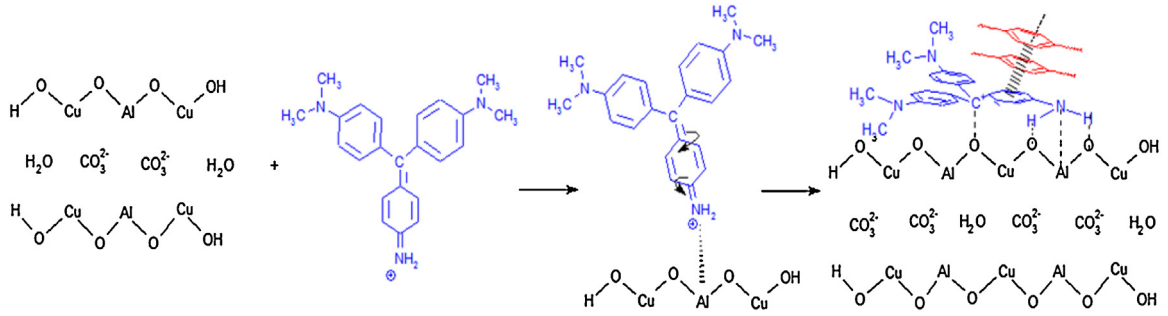

Fig. 6. Interaction mechanism for the adsorption process of MV2B onto LDH Cu/Al.

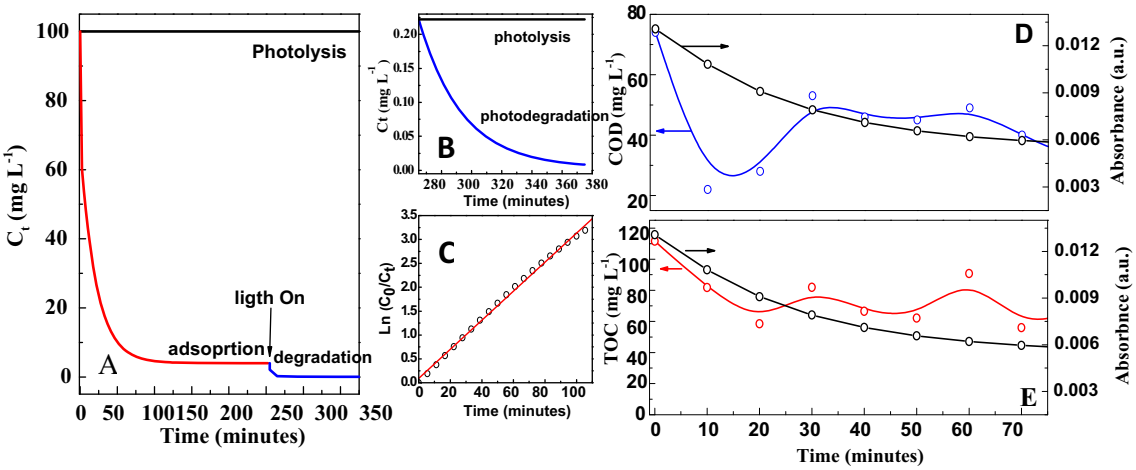

Fig. 7. (A) Sequential adsorption-degradation process as a function of time, (B) degradation of MV2B (light on), (C) pseudo first order kinetics degradation from L–H model, (D) COD removal and (E) TOC measurements. (For interpretation of the references to color in text, the reader is referred to the web version of this article.)

axe of dye molecule is parallel to surface of LDH. Fig. 5E compares UV–vis-NIR spectra of the LDH Cu/Al, after adsorption and MV2B pigment solid samples. The colorant exhibits an absorption broad band between 300 and 750 nm, the electronic transitions observed in colored solution are no evident, while for the sample after MV2B adsorption the electronic transitions are clearly observed, suggesting that exists also the interaction between the colorant and the adsorbed water or OH of LDH. It seems that unbounded electron pair of amino group of dye interacts with Al^{3+} centers (of LDH) leading to the delocalization of π electrons in the double bonds C=N and C=C.

^{13}C RMN results (Fig. 5F) are in line with discussion above described. It is evident that dislocation of π electrons results in a variation of relative intensities of NMR signals as the local electronic environment changing the relaxation time of signal. Note that signals the most modified are that close to polar groups (amines), which are the ones expected to interact with the surface of LDH.

The high adsorption capacity of LDH Cu-Al can be attributed to the stacking of colorant in layers by the π–π interactions from the aromatic rings; the adsorption mechanism proposed are exhibited in Fig. 6.

3.4. Photocatalysis

In order to evaluate the photocatalytic activity of LDH Cu/Al, adsorption experiment in dark condition for 265 min was performed (Fig. 7A red line), the uptake of approximately 95% of the molecules in solution (100 mg L^{-1} of MV2B) was noticed after 100 min. It could be seen that an equilibrium adsorption of MV2B was reached within 150 min. After 265 min the solution was stirred under UV light irradiation in order to start the photocatalytic reaction (Fig. 7A blue line), after 100 min of irradiation the 100% removal of MV2B was achieved, whereas by photolysis using a concentration of MV2B of 0.25 mg L^{-1}, the colorant degradation was not evident, verifying that the process is attributed to the photocatalytic activity of LDH Cu/Al (Fig. 7B).

The kinetic data of photodegradation mediate by LDH Cu/Al was analyzed as a simple rate expression of Langmuir–Hinshelwood (L–H) model [49]:

$$\ln\left(\frac{C_t}{C_0}\right) = k_{ap}t \tag{11}$$

Yielding half-life, $t_{1/2}$ (in min) as:

$$t_{1/2} = \frac{0.693}{k_{ap}} \tag{12}$$

where k_{ap} is the apparent reaction rate constant and t is the reaction time. Rate constant k_{ap} independent of used concentration can be determined from the slope of the curve $\ln C_t/C_0$ versus t (Fig. 7C). The linearity of the curves indicates that the kinetics for the photocatalytic decomposition of MV2B follows pseudo-first-order rate. The apparent decomposition rate constant was 0.00314 min^{-1} ($t_{1/2}$ = 220 min).

To confirm the photo-degradation of MV2B, parameters as chemical oxygen demand (COD) and total organic carbon (TOC) were related to the absorbance, which also was measured during the evolution of photocatalytic reaction (Fig. 7D and E, respectively). Clearly, the absorbance in both analyses decreased, confirming that the colorant is not present in solution otherwise the absorbance values were higher, while the TOC and DQO profiles are complexes. This behavior can be explained due to the occurrence of

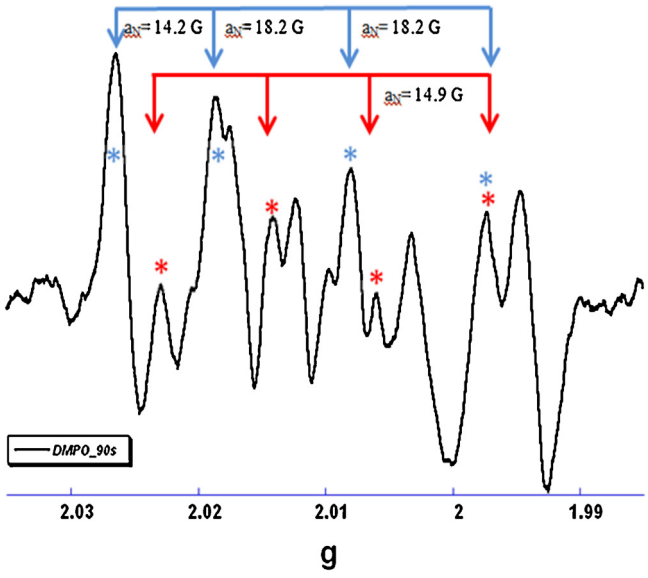

Fig. 8. EPR spectra of DMPO/•OH and DMPO/•OOH adducts formed during the photodegradation. (For interpretation of the references to color in text, the reader is referred to the web version of this article.)

simultaneous processes, one of them is associated to the desorption of degradation products from MV2B.

On the other hand, the detection of several radicals by EPR spin trapping with DMPO (this has been widely used to trap •OH in biological systems as the DMPO–OH adduct) were tested in a system containing 50 mM DMPO [50], LDH Cu/Al and solution containing dye in the presence of UV light for a period of 90 s. An intense EPR signals exhibit the formation of various radicals that could be associated with formation of superoxide and hydroxyl radicals and other organic radicals [51]. The most intense signals were assigned to a DMPO/•OH complex (a^N = 14.2 Gauss), which had a relative intensity of 1:2:2:1 as shown in Fig. 8(red mark). Another specie founded in solution was the superoxide radical, as is showed in the Fig. 8 (blue mark), with values of DMPO/•OOH adduct, a^N = 14.2 and 18.2 Gauss. These results were reproducible in a repetition of the experiment.

EPR spectra show that hydroxyl radical, superoxide radical and other carbon centered radical were observed in solution, but superoxide founded has less concentration, due to this radical is formed first, and the hydroxyl formed is part of the decay of superoxide. DMPO/•OH adduct has a half-life in the range of 12–156 min in neutral solutions. Hydroxyl radicals (•OH) in the presence of dissolved molecular oxygen is converted into the superoxide anion ($^{\bullet}O_2^-$) [52].

These data confirm presence of several radicals in solution and they are the support for describe a mechanism that includes the formation at least two species, hydroxyl and superoxide radicals. The hydroxyl radical has been known that promotes the degradation of organic matter and thus be useful for improving the quality of water contaminated with dyes. In the spectra appeared other signals that can be assigned to another organic radical from products of decomposition of dye as shown in the next scheme [53].

$$\text{Catalyst} + h\upsilon \rightarrow \text{Catalyst}(e^- + h^+)$$

$$\text{Catalyst}(h^+) + H_2O \rightarrow \text{Catalyst} + H^+ + {}^{\bullet}OH$$

$$\text{Dye} + {}^{\bullet}OH \rightarrow CO_2$$

$$\text{Catalyst}(e^-) + O_2 \rightarrow \text{Catalyst} + O_2^{-\cdot}$$

$$O_2^{-\cdot} + \text{dye} \rightarrow \text{Products from dyes}$$

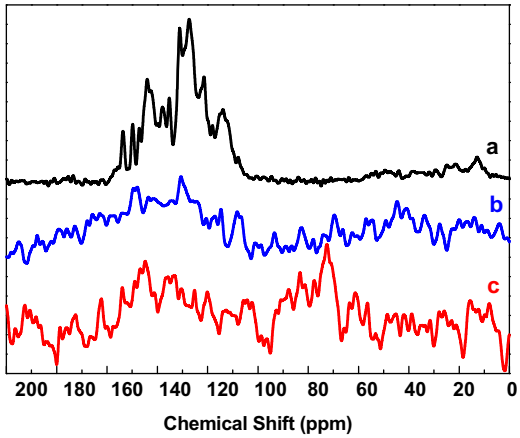

Fig. 9. ^{13}C NMR spectra of (a) MV2B dye, MV2B adsorbed on LDH Cu/Al: (b) before and (c) after photodegradation.

Fig. 9 compares the ^{13}C NMR MAS spectra of pure dye, adsorbed dye on LDH and dye after adsorption and subsequent photocatalysis. Significant changes regarding the aromatic carbons are observed. The pure dye shows intense signals within 100–170 ppm range but the signal intensity decreased significantly upon dye adsorption with is explained because the low amount of dye adsorbed and also because the change in the relaxation of signals as explained above. With photocatalysis the spectrum is again modified, evidencing signals at stronger field, actually the signal close to ppm is hard to assign to carbon bonded to nitrogen coming from amine group, rather match with a carbon bonded to nitrogen of a nitro group. It seems then that also the NH_2 group is oxidized to NO_2.

4. Conclusions

LDH Cu/Al material was prepared by coprecipitation method; the structure was confirmed by XRD and FTIR analyses. Adsorption of MV2B dye process was described using Langmuir, Freundlich and Temkin models, from this, high adsorption capacity in the value of 361.0 mg g^{-1} was obtained, associated to the physisorption thermodynamically stable, the kinetics fitted to the pseudo-second order mechanism. The high adsorption capacity of LDH Cu-Al can be attributed to the stacking of colorant in layers by the π–π interactions from the aromatic rings, more than 90% of the dissolved MV2B was removed in the firsts 15 min. LDH Cu/Al showed photoabsorption characteristics giving an optical bandgap E_g = 2.85 eV; this propriety was evaluated in the photodegradation using UV power source after adsorption equilibrium, the degradation process was confirmed by the presence of radicals detected using spin trapping technique (EPR) and the evolution of COD and TOC parameters. The reaction degradation kinetics for the photocatalytic decomposition of MV2B follows pseudo-first-order rate, the apparent decomposition rate constant was 0.00314 min^{-1} and $t_{1/2}$ = 220 min. Important characteristics were detected by ^{13}C NMR MAS for the adsorbed and after degradation samples.

Acknowledgments

Projects: CONACYT INFRA 2014 225161, SIP-IPN 20150898.

References

[1] V. Golob, A. Vinder, M. Simonic, Efficiency of the coagulation/flocculation method for the treatment of dye bath effluents, Dyes Pigments 67 (2005) 93–97.
[2] W. Herbst, K. Hunger, Industrial Organic Pigments, Wiley-VCH Verlag & Co., Weinheim, Germany, 2004.

[3] M.M. El-Molla, R. Schneider, Development of ecofriendly binders for pigment printing of all types of textile fabrics, Dyes Pigments 71 (2006) 130–137.
[4] J.-S. Wu, C.-H. Liu, K.H. Chu, S.-Y. Suen, Removal of cationic dye methyl violet 2B from water by cation exchange membranes, J. Membr. Sci. 309 (2008) 239–245.
[5] B.H. Hameed, Equilibrium and kinetic studies of methyl violet sorption by agricultural waste, J. Hazard. Mater. 154 (2008) 204–212.
[6] G. Vinitha, A. Ramalingam, Spectral characteristics and nonlinear studies of methyl violet 2B dye in liquid solid media, Laser Phys. 18 (2008) 37–42.
[7] Ö. Güllü, M. Çankaya, M. Bider, A.J. Türüt, Gamma irradiation-induced changes at the electrical characteristics of organic-based Schottky structures, J. Phys. D: Appl. Phys. 41 (2008) 135103–135109.
[8] C. Bouasla, M.E.-H. Samar, F. Ismail, Degradation of methyl violet 6B dye by the Fenton process, Desalination 254 (2010) 35–41.
[9] A. Haldar, S. Maity, N.B. Manik, Effect of back electrode on photovoltaic properties of crystal-violet-dye-doped solid-state thin film, Ionics 14 (2008) 427–432.
[10] A.B.d. Santos, F.J. Cerantes, J.B.v. Lier, Review paper on current technologies for decolourisation of textile wastewaters: perspectives for anaerobic biotechnology, Bioresour. Technol. 98 (2007) 2369–2385.
[11] K.A. Gallagher, M.G. Healy, S.J. Allen, Biosorption of synthetic dye and metal ions from aqueous effluents using fungal biomass: studies in environmental science, in: Proceedings of the 3rd Biennial Meeting of the International Society for Environmental Biotechnology, Global Environmental Biotechnology, Elsevier, 1997.
[12] Y.S. Ho, C.C. Chiang, Sorption studies of acid dye by mixed sorbents, Adosrption 7 (2001) 139–147.
[13] N. Dizge, C. Ayiner, E. Demirbas, M. Kobya, S. Kara, Adsorption of reactive dyes from aqueous solutions by fly ash: kinetic and equilibrium studies, J. Hazard. Mater. 150 (2008) 737–746.
[14] J. Flores, E. Lima, M. Maubert, E. Aduna, J.L. Rivera, Clean-up of wastes from the textile industry using anionic clays, Clays Clay Miner. 59 (2011) 240–249.
[15] R. Hoppe, G. Schulz-Ekloff, D. Wohrle, C. Kirschhock, H. Fuess, Synthesis, location, and photoinduced transformation of zeolite-encaged thioindigo, Langmuir 10 (1994) 1517–1523.
[16] H. Laguna, S. Loera, I.A. Ibarra, E. Lima, M.A. Vera, V. Lara, Azoic dyes hosted on hydrotalcite-like compounds: non-toxic hybrid pigments, Micropor. Mesopor. Mater. 98 (2007) 234–241.
[17] S. Miyata, The syntheses of hydrotalcite-like compounds and their structures and physico-chemical properties I: the systems Mg^{2+}–$A1^{3+}$–NO_3^-, Mg^{2+}–$A1^{3+}$–Cl^-, Mg^{2+}–$A1^{3+}$–ClO_4^-, Ni^{2+}–$A1^{3+}$–$C1^-$ and Zn^{2+}–$A1^{3+}$–$C1^-$, Clays Clay Miner. 23 (1975) 369–375.
[18] S. Li, H. Qin, R. Zuo, Z. Bai, Tribological performance of Mg/Al/Ce layered double hydroxides nanoparticles and intercalated products as lubricant additives, Appl. Surf. Sci. 353 (2015) 643–650.
[19] E. Lima, M.d.J. Martínez-Ortiz, R.I.G. Reyes, M. Vera, Fluorinated hydrotalcites: the addition of highly electronegative species in layered double hydroxides to tune basicity, Inorg. Chem. 51 (2012) 7774–7781.
[20] M.J. Martínez-Ortiz, D. Tichit, P. Gonzalez, B. Coq, The “one-pot” synthesis of 4-methyl-2-pentanone (methyl isobutyl ketone) from acetone over PdCu catalysts prepared from layered double hydroxides, J. Mol. Catal. A: Chem. 201 (2003) 199–210.
[21] D. Tonelli, E. Scavetta, M. Giorgetti, Layered-double-hydroxide-modified electrodes: electroanalytical applications, Anal. Bioanal. Chem. 405 (2013) 603–614.
[22] M.A. Oliver-Tolentino, J. Vázquez-Samperio, A. Manzo-Robledo, R.G. González-Huerta, J.L. Flores-Moreno, D. Ramírez-Rosales, A. Guzmán-Vargas, An approach to understanding the electrocatalytic activity enhancement by superexchange interaction toward OER in alkaline media of Ni–Fe LDH, J. Phys. Chem. C 118 (2014) 22432–22438.
[23] Y. Dou, T. Pan, A. Zhou, S. Xu, X. Liu, J. Han, M. Wei, D.G. Evans, X. Duan, Reversible thermally-responsive electrochemical energy storage based on smart LDH@P(NIPAM-co-SPMA) films, Chem. Commun. 49 (2013) 8462–8464.
[24] G. Chen, S. Qian, X. Tu, X. Wei, J. Zou, L. Leng, S. Luo, Enhancement photocatalytic degradation of rhodamine B on nanoPt intercalated Zn–Ti layered double hydroxides, Appl. Surf. Sci. 293 (2014) 345–351.
[25] Y. Sun, J. Zhou, W. Cai, R. Zhao, J. Yuan, Hierarchically porous NiAl-LDH nanoparticles as highly efficient adsorbent for p-nitrophenol from water, Appl. Surf. Sci. 349 (2015) 897–903.
[26] F. Wu, J. Liang, Z. Peng, B. Liu, Electrochemical deposition and characterization of Zn–Al layered double hydroxides (LDHs) films on magnesium alloy, Appl. Surf. Sci. 313 (2014) 834–840.
[27] M. Zhou, X. Pang, L. Wei, K. Gao, Insitu grown superhydrophobic Zn–Al layered double hydroxides films on magnesium alloy to improve corrosion properties, Appl. Surf. Sci. 337 (2015) 172–177.
[28] J. Hu, M. Gan, L. Ma, J. Zhang, S. Xie, F. Xu, J.Z.X. Shen, H. Yin, Preparation and enhanced properties of polyaniline/grafted intercalated ZnAl–LDH nanocomposites, Appl. Surf. Sci. 328 (2015) 325–334.
[29] F. Márquez, A.E. Palomares, F. Rey, A. Corma, Characterisation of the active copper species for the NO_x removal on Cu/Mg/Al mixed oxides derived from hydrotalcites: an in situ XPS/XAES study, J. Mater. Sci. 11 (2001) 1675–1680.
[30] R. Trujillano, M.J. Holgado, F. Pigazo, V. Rives, Preparation, physicochemical characterisation and magnetic properties of Cu–Al layered double hydroxides with CO_3^{2-} and anionic surfactants with different alkyl chains in the interlayer, Physica B 373 (2006) 267–273.
[31] S. Chakraborty, I. Sarkar, K. Haldar, S.K. Pal, S. Chakraborty, Synthesis of Cu–Al layered double hydroxide nanofluid and characterization of its thermal properties, Appl. Clay Sci. 107 (2015) 98–108.
[32] K. Nejati, S. Davary, M. Saati, Study of 2,4-dichlorophenoxyacetic acid (2,4-D) removal by Cu–Fe-layered double hydroxide from aqueous solution, Appl. Surf. Sci. 280 (2013) 67–73.
[33] T. Kameda, T. Uchiyama, T. Yoshioka, Cu–Al layered double hydroxides intercalated with 1-naphthol-3,8-disulfonate and dodecyl sulfate: adsorption of substituted phenols from aqueous media, New J. Chem. 39 (2015) 6315–6322.
[34] L. Tian, Y. Zhao, S. He, M. Wei, X. Duan, Immobilized Cu–Cr layered double hydroxide films with visible-light responsive photocatalysis for organic pollutants, Chem. Eng. J. 184 (2012) 261–267.
[35] N. Ahmed, Y. Shibata, T. Taniguchi, Y. Izumi, Photocatalytic conversion of carbon dioxide into methanol using zinc–copper–M(III) (M = aluminum, gallium) layered double hydroxides, J. Catal. 279 (2011) 123–135.
[36] H.M. Zeyada, M.M. EL-Nahass, I.S. Elashmawi, A.A. Habashi, Annealing temperatures induced optical constant variations of methyl violet 2B thin films manufactured by the spin coating technique, J. Non-Cryst. Solids 358 (2012) 625–636.
[37] C. Loison, R. Antoine, M. Broyer, P. Dugourd, J. Guthmuller, D. Simon, Microsolvation effects on the optical properties of crystal violet, Chem. Eur. J. 14 (2008) 7351–7357.
[38] P. Sahoo, S. Ishihara, K. Yamada, K. Deguchi, S. Ohki, M. Tansho, T. Shimizu, N. Eisaku, R. Sasai, J. Labuta, D. Ishikawa, J.P. Hill, K. Ariga, B.P. Bastakoti, Y. Yamauchi, N. Iyi, Rapid exchange between atmospheric CO_2 and carbonate anion intercalated within magnesium rich layered double hydroxide, ACS Appl. Mater. Interfaces 6 (2014) 18352–18359.
[39] V. Rives, S. Kannan, Layered double hydroxides with the hydrotalcite-type structure containing Cu^{2+}, Ni^{2+} and Al^{3+}, J. Mater. Chem. 10 (2000) 489–495.
[40] A.E. Morales, E.S. Mora, U. Pal, Use of diffuse reflectance spectroscopy for optical characterization of un-supported nanostructures, Rev. Mex. Fis. 53 (2007) 18–22.
[41] P. Wang, Y. Ao, C. Wang, J. Hou, J. Qian, Enhanced photoelectrocatalytic activity for dye degradation by graphene–titania composite film electrodes, J. Hazard. Mater. 223–224 (2012) 78–83.
[42] C.-Y. Kuo, C.-H. Wu, J.-Y. Wu, Adsorption of direct dyes from aqueous solutions by carbon nanotubes: determination of equilibrium, kinetics and thermodynamics parameters, J. Coll. Interface Sci. 327 (2008) 308–315.
[43] A.O. Dada, A.P. Olalekan, A.M. Olatunya, O. Dada, Langmuir, Freundlich, Temkin and Dubinin–Radushkevich isotherms studies of equilibrium sorption of Zn^{2+} unto phosphoric acid modified rice husk, J. Appl. Chem. 3 (2012) 38–45.
[44] M. Dogan, M. Alkan, Adsorption kinetics of methyl violet onto perlite, Chemosphere 50 (2003) 517–528.
[45] S. Azizian, M. Haerifar, H. Bashiri, Adsorption of methyl violet onto granular activated carbon: equilibrium, kinetics and modeling, Chem. Eng. J. 146 (2009) 36–41.
[46] N.B.-H. Abdelkader, A. Bentouami, Z. Derriche, N. Bettahar, L.-C.d. Ménorval, Synthesis and characterization of Mg–Fe layer double hydroxides and its application on adsorption of Orange G from aqueous solution, Chem. Eng. J. 169 (2011) 231–238.
[47] S. Xu, J. Yu, W. Wu, L. Xue, Y. Sun, Synthesis and characterization of layered double hydroxides intercalated by UV absorbents and their application in improving UV aging resistance of bitumen, Appl. Clay Sci. 114 (2015) 112–119.
[48] C.-H. Zhou, J.N. Beltramini, C.-X. Lin, Z.-P. Xu, G.Q.M. Lub, A. Tanksale, Selective oxidation of biorenewable glycerol with molecular oxygen over Cu-containing layered double hydroxide-based catalysts, Catal. Sci. Technol. 1 (2011) 111–122.
[49] J.S. Valente, F. Tzompantzi, J. Prince, J.G.H. Cortez, R. Gomez, Adsorption and photocatalytic degradation of phenol and 2,4 dichlorophenoxiacetic acid by Mg–Zn–Al layered double hydroxides, Appl. Catal. B 90 (2009) 330–338.
[50] E. Finkelstein, G.M. Rosen, E.J. Rauckman, Spin trapping of superoxide and hydroxyl radical: practical aspects, Arch. Biochem. Biophys. 200 (1980) 1–16.
[51] G.M. Rosen, B.E. Britigan, H.J. Helpern, S. Pou, Free radicals. Biology and Detection by Spin Trapping, Oxford University Press, New York, 1999.
[52] G.R. Buettner, Spin trapping: ESR parameters of spin adducts, Free Radic. Biol. Med. 3 (1987) 259–303.
[53] J.L. Clement, N. Ferre, D. Siri, H. Karoui, A. Rockenbauer, P. Tordo, Assignment of the EPR spectrum of 5,5-dimethyl-1-pyrroline N-oxide (DMPO) superoxide spin adduct, J. Org. Chem. 70 (2005) 1198–1203.